The Aeronautical Journal (2024), **128**, pp. 875–895
doi:10.1017/aer.2023.79

REGULAR PAPER

Attitude tracking control of hypersonic vehicle based on an improved prescribed performance dynamic surface control

Z.Y. Yin, B. Wang, R.T. Xiong, Z. Xiang, L. Liu, H.J. Fan and C.L. Xue

National Key Laboratory of Science and Technology on Multispectral Information Processing, School of Artificial Intelligence and Automation, Huazhong University of Science and Technology, Wuhan 430074, China
Corresponding author: B. Wang; Email: wb8517@hust.edu.cn

Received: 8 April 2023; **Revised:** 10 July 2023; **Accepted:** 8 August 2023

Keywords: Hypersonic vehicle; Improved prescribed performance control; Adaptive scaling strategy; Nonlinear disturbance observer

Abstract

In this paper, we investigate the constrained attitude control problem of hypersonic vehicles (HVs). An improved prescribed performance dynamic surface control method is proposed based on an adaptive scaling strategy. Because of the uncertain time-varying disturbances, the controlled state may violate the constraint in the prescribed performance control (PPC) framework. An adaptive scaling strategy is introduced in the PPC method to avoid state violation. The performance function is scaled with respect to the state adaptively. Moreover, a nonlinear disturbance observer is used to compensate the sum of external and other internal disturbances of the system. The proposed method improves the system dynamic performance while ensuring the system robustness. Furthermore, the stability of the closed-loop system is proved by Lyapunov analysis. Finally, numerical simulations are implemented to verify the effectiveness of the PPC method and superiority over other methods.

Abbreviations

AOA	angel-of-attack
BBT	bank to turn
DSC	dynamic surface control
HV	hypersonic vehicles
IPPDSC-NDO	improved prescribed performance dynamic surface control - nonlinear disturbance observer
NDO	nonlinear disturbance observer
PPC	prescribed performance control
PPF	prescribed performance function
PPSMC	prescribed performance sliding mode control

Nomenclature

$C_{L\alpha}$	lift force aerodynamic coefficient related with angle-of-attack
$C_{Y\beta}$	lateral force aerodynamic coefficient related with angle of sideslip
$C_{D\alpha}$	drag force aerodynamic coefficient related with angle-of-attack
$C_{m\alpha}$, C_{mq}	pitch moment aerodynamic coefficient related with angle-of-attack and pitch angular velocity
$C_{n\beta}$, C_{np}, C_{nr}	yaw moment aerodynamic coefficient related with angle of sideslip, roll angular velocity, and yaw angular velocity
$C_{l\beta}$, C_{lp}, C_{lr}	roll moment aerodynamic coefficient related with angle of sideslip, roll angular velocity, and yaw angular velocity

$C_{L\delta_e}, C_{L\delta_a}$	lift force aerodynamic coefficient related with elevons
$C_{Y\delta_e}, C_{Y\delta_a}, C_{Y\delta_r}$	lateral force aerodynamic coefficient related with elevons and rudder
$C_{D\delta_e}, C_{D\delta_a}, C_{D\delta_r}$	drag force aerodynamic coefficient related with elevons and rudder
$C_{m\delta_e}, C_{m\delta_a}$	pitch moment aerodynamic coefficient related with elevons
$C_{n\delta_e}, C_{n\delta_a}, C_{n\delta_r}$	yaw moment aerodynamic coefficient related with elevons and rudder
$C_{l\delta_e}, C_{l\delta_a}, C_{l\delta_r}$	roll moment aerodynamic coefficient related with elevons and rudder
$C^{\delta_e}_{L\delta_e}, C^{\delta_a}_{L\delta_a}$	lift force aerodynamic coefficient derivatives related with elevons
$C^{\delta_e}_{Y\delta_e}, C^{\delta_a}_{Y\delta_a}, C^{\delta_r}_{Y\delta_r}$	lateral force aerodynamic coefficient derivatives related with elevons and rudder
$C^{\delta_e}_{D\delta_e}, C^{\delta_a}_{D\delta_a}, C^{\delta_r}_{D\delta_r}$	drag force aerodynamic coefficient derivatives related with elevons and rudder
$C^{\delta_e}_{m\delta_e}, C^{\delta_a}_{m\delta_a}, C^{\delta_r}_{m\delta_r}$	pitch moment aerodynamic coefficient derivatives related with elevons and rudder
$C^{\delta_e}_{n\delta_e}, C^{\delta_a}_{n\delta_a}, C^{\delta_r}_{n\delta_r}$	yaw moment aerodynamic coefficient derivatives related with elevons and rudder
$C^{\delta_e}_{l\delta_e}, C^{\delta_a}_{l\delta_a}, C^{\delta_r}_{l\delta_r}$	roll moment aerodynamic coefficient derivatives related with elevons and rudder

1.0 Introduction

In recent years, HVs have been gradually widely used in military, civil, and other fields. Their main feature is the fast speed. The fastest cruising speed can reach Mach 15–20, which can achieve rapid attack on enemy targets. Because of their high penetration ability and other superior performance, many countries are scrambling to invest a lot of funds and personnel for research. Although HVs have many superior performances, they also have many control technology problems compared with ordinary vehicles, such as large flight envelope and complex flight environment. Therefore, there will be uncertainties in aerodynamic parameters. Moreover, the HV model has strong coupling and strong nonlinearity. These problems will bring many new challenges to flight control technology [1, 2].

At present, scholars have proposed various tracking control methods for high-speed aircraft. A backstepping method combined with the nonlinear disturbance observer is proposed to realise the auto-disturbance rejection control of HVs [3]. An anti-saturation controller based on the backstepping method and sliding mode theory is proposed to complete the control of HVs [4]. A robust adaptive controller based on backstepping method is designed to overcome actuator saturation in HVs while achieving good control effect [5]. A high-order sliding mode control based on feedback linearisation is proposed to improve the controller's robustness of HVs while eliminating chattering [6]. An integral sliding mode control method is proposed to solve the problem of external disturbance in HVs tracking process [7, 8]. A control method based on nonlinear disturbance observer is proposed to deal with the disturbance problems in the tracking control process of HVs [9]. A fault-tolerant control method based on fast fault observer is proposed to solve the problem of fault for HVs [10]. A smooth adaptive terminal sliding-mode-based controller is proposed for bank-to-turn (BTT) missiles [11]. A robust approximate optimal controller based on adaptive dynamic programming is proposed, aiming to drive the HVs with uncertainties to follow the virtual command [12]. The above methods have achieved good control performance, but they don't consider the problem of the system dynamic performance.

Scholars pay more attention to the dynamic performance in the tracking process besides the tracking stability of HV in recent years. The PPC method is a pre-designed transient performance parameters method. It has good compatibility with other control methods [13], which can better ensure the control performance of the system. The concept of prescribed performance and funnel control method are proposed by Ilchmann [14]. The PPC method proposed by Bechlioulis and Rovithakis further improves the versatility of this method [13]. Since then, the PPC method has received widespread attention. Because of its good dynamic performance, it is gradually applied to high-precision controllers of aerospace vehicles [15–17]. Since the PPC method is to restrict the related state, it increases the design difficulty of the related controller. In general, we can design a function to constrain the state. This method can convert the constrained state into the new unconstrained state under the homeomorphism mapping. Meanwhile, it can reduce the design difficulty of the controller [18, 19].

In addition, the PPC method generally has a problem that the state may violate the constraint. If the state violation occurs, it will lead to a computational singularity, even a divergence of the system. Some

https://doi.org/10.1017/aer.2023.79 Published online by Cambridge University Press

new forms of prescribed performance function (PPF) in terms of the initial value and convergence time are proposed [20–24], but the problem of state violation is not considered.

Based on the above analysis, this paper proposes an improved prescribed performance dynamic surface control method with an adaptive scaling strategy, aiming to realise the constrained attitude control of HVs with uncertain disturbances. The key idea of this paper is to propose an adaptive scaling strategy and a nonlinear disturbance observer into the PPC framework based on the dynamic surface control method. This combined control method can achieve not only the fast convergence of the system's tracking error according to the prescribed performance, but also quick estimation and compensation of the disturbance to enhance the system's anti-disturbance ability. Besides, it can avoid the state violation. The contributions of this paper are as follows :

(1) Based on an adaptive scaling strategy, an adaptive prescribed performance function is proposed. The PPF can scale adaptively based on relevant state if the state violates the constraint. The strategy can avoid the state violation. Furthermore, it can avoid a computational singularity and the corresponding system divergence problem. Besides, we set some PPF structure parameters according to the initial state error. It can make the parameter setting more flexible. In summary, it can not only retain the advantage of PPC excellent dynamic performance, but also avoid the problems caused by the state violation.

(2) The method of combining the PPC method and the dynamic surface control is adopted in this paper to realise the design of the controller. It plays a role in enhancing system dynamic performance. Meanwhile, a first-order filter is introduced to solve the problem of 'explosion of terms' in the traditional backstepping control. Furthermore, a nonlinear disturbance observer is introduced into the PPC framework, which makes up for the lack of system robustness. Finally, numerical simulations are implemented to verify the effectiveness of the combined control method.

(3) For the constrained attitude control problem in this paper, by choosing the appropriate Lyapunov function, the stability of the designed controller is proved. Furthermore, the constrained state satisfies the PPF constraint we designed.

The organisational structure of this paper is as follows: in the second section, we give the modeling assumptions and modeling process. The third section provides the controller design method and stability proof based on the prescribed performance backstepping control. In the fourth section, the simulations of tracking control are given, which verify the advantages of the control method. Finally, the method is summarised in the fifth section.

2.0 Formulation

The tapered general-purpose winged-cone [25] is taken as the research object. The overall shape of the winged-cone is a cone-shaped structure. Its front view and side view are shown in Fig. 1.

The front of the wing cone is equipped with canard wings, which can only be opened when flying at low speed (subsonic state). When entering hypersonic flight, the canard will be inserted into the belly of the wing cone to improve flight speed. When the winged-cone re-enters the atmosphere, the engine shuts down and the flight only depends on elevons and rudder control to glide in the atmosphere.

Before establishing the HV dynamical model, we need to make corresponding assumptions according to the flight characteristics of the HV to facilitate our subsequent modeling:

Assumption 1. *Ignore the impact of the Earth's rotation and treat the Earth as a sphere.*

Assumption 2. *Ignore the elastic characteristics of the body, wing and rudder surface, and consider the HV as an ideal rigid body with uniform mass distribution.*

Assumption 3. *Ignore the impact of liquid fuel sloshing in the HV, and the mass of HV is considered constant.*

https://doi.org/10.1017/aer.2023.79 Published online by Cambridge University Press

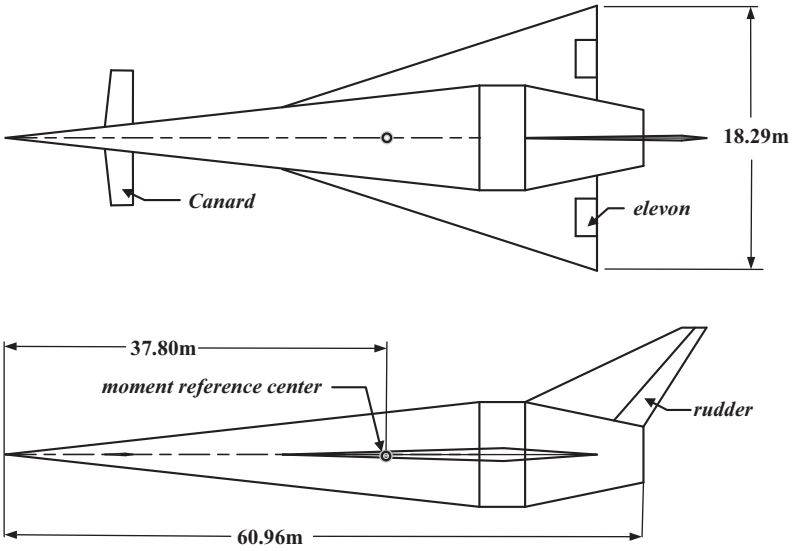

Figure 1. *Front and side views of the winged-cone.*

In the reentry attitude control problem of the HV, we tend to pay the most attention to two groups of states. They are attitude angle $\theta = (\alpha, \beta, \mu)^T$ and attitude angular velocity $\omega = (q, r, p)^T$. The nonlinear dynamical model of the HV used in this paper can be written as follows [25]:

$$\begin{aligned}
\dot{\alpha} &= q - \tan\beta(p\cos\alpha + r\sin\alpha) + \frac{-L + m_0 g\cos\gamma\cos\mu}{m_0 V\cos\beta} + d_\alpha \\
\dot{\beta} &= p\sin\alpha - r\cos\alpha + \frac{Y + m_0 g\cos\gamma\sin\mu}{m_0 V} + d_\beta \\
\dot{\mu} &= \frac{p\cos\alpha + r\sin\alpha}{\cos\beta} + \frac{L(\tan\beta + \tan\gamma\sin\mu) + Y\tan\gamma\cos\mu - m_0 g\cos\gamma\tan\beta\cos\mu}{m_0 V} + d_\mu \\
\dot{q} &= \frac{J_z - J_x}{J_y}pr + \frac{m + x_{cg}(D\sin\alpha + L\cos\alpha)}{J_y} + d_q \\
\dot{r} &= \frac{J_x - J_y}{J_z}pq + \frac{n - x_{cg}Y}{J_z} + d_r \\
\dot{p} &= \frac{J_y - J_z}{J_x}qr + \frac{l}{J_x} + d_p
\end{aligned} \tag{1}$$

where, α, β, μ respectively represent the angle-of-attack, angle of sideslip and angle of bank. q, r, p respectively represent the angular rates of pitch, yaw and roll. γ represents flight path angle. J_x, J_y, J_z are the rotational inertias of the body around three axes respectively. m_0 and V are the mass and velocity of the HV respectively. x_{cg} represents the distance from the pressure centre to the mass center. L, Y, D are the lift, lateral and drag force of the HV respectively. m, n, l are the pitch, yaw and roll moment of the HV respectively. d_α, d_β, d_μ are the equivalent disturbance force of the HV model's each channel respectively. d_q, d_r, d_p are the equivalent disturbance moment of the HV model's each channel respectively. $g = g_0\left(\frac{R_e}{R_e + H}\right)^2$, g_0 is acceleration of gravity on the earth's surface, R_e is Earth radius, H is the flight altitude.

https://doi.org/10.1017/aer.2023.79 Published online by Cambridge University Press

The aerodynamic forces and aerodynamic moments of the HV are expressed as follows :

$$\begin{aligned} L &= C_L \bar{q} S \\ m &= C_m \bar{q} c S \\ Y &= C_Y \bar{q} S \\ n &= C_n \bar{q} b S \\ D &= C_D \bar{q} S \\ l &= C_l \bar{q} b S \end{aligned} \tag{2}$$

where, C_i $(i = L, Y, D, m, n, l)$ represents the relevant force aerodynamic and moment aerodynamic coefficient. $\bar{q}, c, b, S$ are the dynamic pressure, reference aerodynamic chord, wing span and reference area of the HV respectively. Besides, $\bar{q} = \frac{1}{2}\rho V^2$, $\rho = \rho_0 e^{-\frac{H}{H_0}}$, where ρ is atmospheric density, ρ_0 is atmospheric density on the earth's surface, H_0 is equivalent atmospheric scale height.

The aerodynamic coefficients' composition are as follows [25]:

$$\begin{aligned} C_L &= C_{L\alpha} + C_{L\delta_e} + C_{L\delta_a} \\ C_Y &= C_{Y\beta} + C_{Y\delta_e} + C_{Y\delta_a} + C_{Y\delta_r} \\ C_D &= C_{D\alpha} + C_{D\delta_e} + C_{D\delta_a} + C_{D\delta_r} \\ C_m &= C_{m\alpha} + C_{m\delta_e} + C_{m\delta_a} + C_{m\delta_r} + C_{mq}\frac{qc}{2V} \\ C_n &= C_{n\beta}\beta + C_{n\delta_e} + C_{n\delta_a} + C_{n\delta_r} + C_{np}\frac{pb}{2V} + C_{nr}\frac{rb}{2V} \\ C_l &= C_{l\beta}\beta + C_{l\delta_e} + C_{l\delta_a} + C_{l\delta_r} + C_{lp}\frac{pb}{2V} + C_{lr}\frac{rb}{2V} \end{aligned} \tag{3}$$

where, δ_e, δ_a, δ_r represent the left elevon angle, the right elevon angle and the rudder angle respectively.

The final actual control are the deflection angles of the HV. The control input is defined as $U = (\delta_e, \delta_a, \delta_r)^T$. In order to facilitate the subsequent controller design, Equation (1) is further sorted and rewritten into an affine nonlinear form (without disturbances):

$$\begin{aligned} \dot{\theta} &= B_\delta g_{s\delta} U + f_s(\theta) + g_s \omega \\ \dot{\omega} &= J^{-1} g_{f\delta} U + f_f(\omega) \end{aligned} \tag{4}$$

where, $J^{-1} = diag\{J_y^{-1}, J_z^{-1}, J_x^{-1}\}$. B_δ is the equivalent control force efficiency matrix. g_s represents the system state matrix of angle loop. The specific expression of matrix B_δ and g_s are shown in Equations (5 and 6):

$$B_\delta = \frac{1}{m_0 V}\begin{pmatrix} \frac{1}{\cos\beta} & 0 & 0 \\ 0 & 1 & 0 \\ 0 & 0 & 1 \end{pmatrix} \tag{5}$$

$$g_s = \begin{pmatrix} 1 & -\sin\alpha\tan\beta & -\cos\alpha\tan\beta \\ 0 & -\cos\alpha & \sin\alpha \\ 0 & \sin\alpha\sec\beta & \cos\alpha\sec\beta \end{pmatrix} \tag{6}$$

where, $f_s(\omega) = \begin{pmatrix} f_\alpha & f_\beta & f_\mu \end{pmatrix}^T$ is a vector function of attitude angle. $f_f(\omega) = \begin{pmatrix} f_q & f_r & f_p \end{pmatrix}^T$ is a vector function of attitude angular velocity. The specific expression of vector function $f_s(\omega)$ and $f_f(\omega)$ are shown in Equations (7 and 8):

https://doi.org/10.1017/aer.2023.79 Published online by Cambridge University Press

$$
\begin{aligned}
f_\alpha &= \frac{-C_{L\alpha}\bar{q}S + m_0 g\cos\gamma\cos\mu}{m_0 V\cos\beta} \\
f_\beta &= \frac{-C_{Y\beta}\bar{q}S + m_0 g\cos\gamma\sin\mu}{m_0 V} \\
f_\mu &= \frac{C_{Y\beta}\bar{q}S\cos\mu + C_{L\alpha}\bar{q}S\sin\mu}{m_0 V}\tan\gamma + \frac{C_{L\alpha}\bar{q}S - m_0 g\cos\gamma\cos\mu}{m_0 V}\tan\beta
\end{aligned} \tag{7}
$$

$$
\begin{aligned}
f_q &= \frac{J_z - J_x}{J_y}pr + \frac{\bar{q}cS\left(C_{m\alpha} + C_{mq}\dfrac{qc}{2V}\right) + x_{cg}\bar{q}S(C_{D\alpha}\sin\alpha + C_{L\alpha}\cos\alpha)}{J_y} \\
f_r &= \frac{J_x - J_y}{J_z}pq + \frac{\bar{q}bS\left(C_{n\beta} + C_{np}\dfrac{pb}{2V} + C_{nr}\dfrac{rb}{2V}\right) - x_{cg}\bar{q}S\,C_{Y\beta}}{J_z} \\
f_p &= \frac{J_y - J_z}{J_x}qr + \frac{\bar{q}bS\left(C_{l\beta} + C_{lp}\dfrac{pb}{2V} + C_{lr}\dfrac{rb}{2V}\right)}{J_x}
\end{aligned} \tag{8}
$$

where, $g_{s\delta}$ is the control matrix generated by deflection angle to attitude angle. $g_{f\delta}$ is the control matrix generated by deflection angle to attitude angular velocity. The specific expressions of matrix $g_{s\delta}$ and $g_{f\delta}$ are shown in Equations (9 and 10):

$$
g_{s\delta} = \bar{q}s\begin{pmatrix} g_{\alpha\delta_e} & g_{\alpha\delta_a} & g_{\alpha\delta_r} \\ g_{\beta\delta_e} & g_{\beta\delta_a} & g_{\beta\delta_r} \\ g_{\mu\delta_e} & g_{\mu\delta_a} & g_{\mu\delta_r} \end{pmatrix} \tag{9}
$$

$$
g_{f\delta} = \bar{q}s\begin{pmatrix} g_{q\delta_e} & g_{q\delta_a} & g_{q\delta_r} \\ g_{r\delta_e} & g_{r\delta_a} & g_{r\delta_r} \\ g_{p\delta_e} & g_{p\delta_a} & g_{p\delta_r} \end{pmatrix} \tag{10}
$$

Equation (11) is the specific expression of variables in Equations (9 and 10):

$$
\begin{aligned}
&g_{\alpha\delta_e} = -C^{\delta_e}_{L\delta_e};\ g_{\beta\delta_e} = C^{\delta_e}_{Y\delta_e};\ g_{\mu\delta_e} = C^{\delta_e}_{Y\delta_e}\tan\gamma\cos\mu + C^{\delta_e}_{L\delta_e}(\tan\gamma\sin\mu + \tan\beta); \\
&g_{\alpha\delta_a} = -C^{\delta_a}_{L\delta_a};\ g_{\beta\delta_a} = C^{\delta_a}_{Y\delta_a};\ g_{\mu\delta_a} = C^{\delta_a}_{Y\delta_a}\tan\gamma\cos\mu + C^{\delta_a}_{L\delta_a}(\tan\gamma\sin\mu + \tan\beta); \\
&g_{\alpha\delta_r} = 0;\ g_{\beta\delta_r} = C^{\delta_r}_{Y\delta_r};\ g_{\mu\delta_r} = C^{\delta_r}_{Y\delta_r}\tan\gamma\cos\mu; \\
&g_{q\delta_e} = cC^{\delta_e}_{m\delta_e} + x_{cg}\left(C^{\delta_e}_{D\delta_e}\sin\alpha + C^{\delta_e}_{L\delta_e}\cos\alpha\right);\ g_{r\delta_e} = bC^{\delta_e}_{n\delta_e} - x_{cg}C^{\delta_e}_{Y\delta_e};\ g_{p\delta_e} = bC^{\delta_e}_{l\delta_e}; \\
&g_{q\delta_a} = cC^{\delta_a}_{m\delta_a} + x_{cg}\left(C^{\delta_a}_{D\delta_a}\sin\alpha + C^{\delta_a}_{L\delta_a}\cos\alpha\right);\ g_{r\delta_a} = bC^{\delta_a}_{n\delta_a} - x_{cg}C^{\delta_a}_{Y\delta_a};\ g_{p\delta_a} = bC^{\delta_a}_{l\delta_a}; \\
&g_{q\delta_r} = cC^{\delta_r}_{m\delta_r} + x_{cg}C^{\delta_r}_{D\delta_r}\sin\alpha;\ g_{r\delta_r} = bC^{\delta_r}_{n\delta_r} - x_{cg}C^{\delta_r}_{Y\delta_r};\ g_{p\delta_r} = bC^{\delta_r}_{l\delta_r};
\end{aligned} \tag{11}
$$

The $B_\delta g_{s\delta}U$ and $f_s(\theta)$ in the Equation (4) are small quantities, and consider the existence of disturbances and unmodeled dynamics. In order to facilitate the subsequent controller design, Equation (4) is further rewritten. These small quantities and unmodeled dynamics are treated as internal disturbances of the model, and the final affine nonlinear model can be written as follows :

$$
\begin{aligned}
\dot{\theta} &= g_s\omega + \Delta_s \\
\dot{\omega} &= g_f U + f_f(\omega) + \Delta_f
\end{aligned} \tag{12}
$$

https://doi.org/10.1017/aer.2023.79 Published online by Cambridge University Press

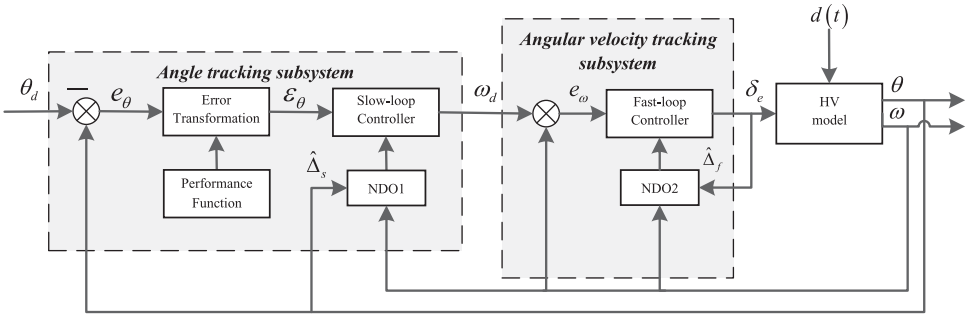

Figure 2. *Control system structure block diagram.*

where, $g_f = J^{-1}g_{f\delta}$. $\Delta_s = B_\delta g_{s\delta}U + f_s(\theta) + D_1$. $\Delta_f = J^{-1}M_\delta + D_2$. D_1 and D_2 are the sum of external disturbances and other internal disturbances such as system uncertainty and unmodeled dynamics, $D_1, D_2 \in R^{3\times 1}$.

3.0 Controller design

3.1 Prescribed performance control structure

The design method of the prescribed performance controller is as follows. First, the PPF is designed to constrain the state, and then the corresponding control strategy is proposed for the constrained state. The control performance of the system can be guaranteed. In order to obtain the better comprehensive performance of angle tracking control, the PPC structure is adopted in the outer loop. The error transformation function in the outer loop is used to transform the actual control error into virtual error. Then a dynamic surface controller is designed for the virtual error to ensure the boundedness of the transformed system error. Finally, design the relevant dynamic surface controller in the inner loop.

In this section, the method of unconstrained translation of state under homeomorphic mapping is adopted. It can transform the constrained state control problem into a new unconstrained state control problem. The whole system control structure is shown in Fig. 2.

3.1.1 General PPF and error transformation form

The controlled state is generally taken as error $e(t)$ in the prescribed performance tracking control. In most current researches related to the PPC method [26–28], the PPF is usually used:

$$\rho(t) = k(\rho_0 - \rho_\infty)\, e^{-\lambda t} + \rho_\infty \tag{13}$$

where, ρ_0 represents the initial error limit, ρ_∞ represents the steady-state error limit, λ represents the error convergence rate limit, which can be designed manually. $\rho(t)$ satisfies $\lim_{t\to\infty}\rho(t) = \rho_\infty$ with $\rho_0 > \rho_\infty > 0$. k is the scaling coefficient, and the default value is 1. Then, $e(t)$ satisfies:

$$-L\rho(t) \le e_i(t) \le U\rho(t) \tag{14}$$

Generally, the unconstrained error transformation function is chosen as follows:

$$\begin{aligned} \varepsilon_i(t) &= \frac{1}{2}\ln\left(\frac{LU + Ux_i(t)}{LU - Lx_i(t)}\right) \\ x_i(t) &= \frac{e_i(t)}{\rho(t)} \end{aligned} \tag{15}$$

where, $\varepsilon_i(t) \in R(i = 1, 2, 3)$ is the unconstrained virtual error after conversion. $e_i(t) \in R(i = 1, 2, 3)$ is the actual error.

https://doi.org/10.1017/aer.2023.79 Published online by Cambridge University Press

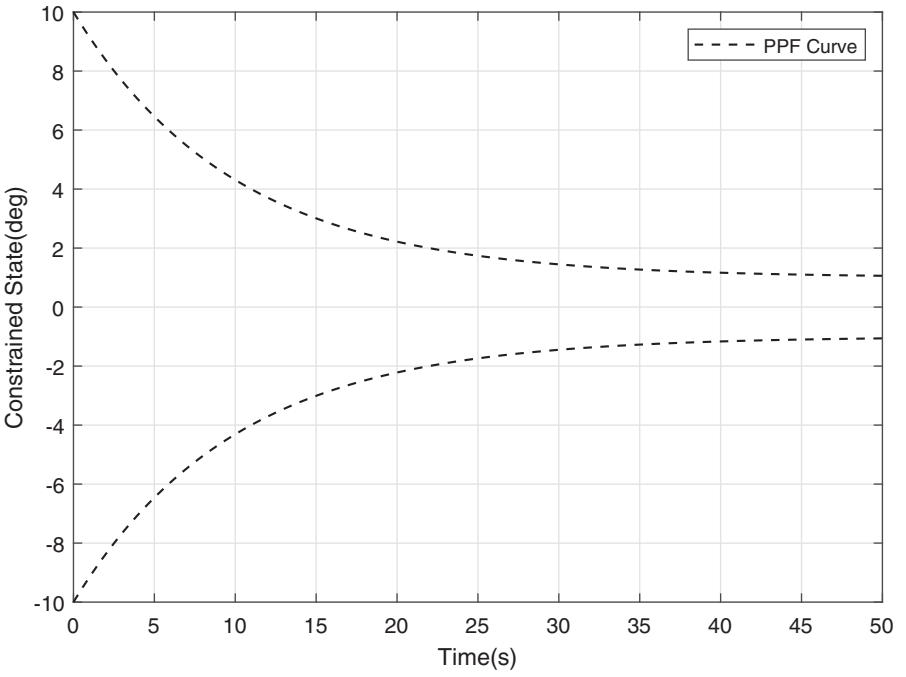

Figure 3. *PPF curve.*

In view of the Equation (15), taking the derivative of $\varepsilon(t) = [\varepsilon_1(t), \varepsilon_2(t), \varepsilon_3(t)]^T$ with respect to time, we can obtain

$$\dot{\varepsilon}(t) = T_d \dot{e}(t) + T_c \tag{16}$$

$$T_{di} = \frac{\dfrac{1}{x_i(t) + L} - \dfrac{1}{x_i(t) - U}}{2\rho(t)} \ (i = 1, 2, 3) \tag{17}$$

$$T_{ci} = -T_{di} \frac{e_i(t)\, \dot{\rho}(t)}{\rho(t)} \ (i = 1, 2, 3) \tag{18}$$

where, $T_d = diag(T_{d1}, T_{d2}, T_{d3})$, $T_c = [T_{c1}, T_{c2}, T_{c3}]^T$. L and U represent the upper and lower error overshoot constraint coefficients, with the range of (0, 1). An example of PPF curve form is shown in Fig. 3 ($L = U = 1$).

3.1.2 PPF with adaptive scaling strategy

Due to the disturbances of the system and drastic changes of reference command, the tracking error may suddenly become large and violate the constraint. In Equation (15), the unconstrained virtual state will result in a computational singularity, even a system divergence caused by the error violation. Therefore, this section proposes a PPC method with an adaptive scaling strategy. The scheme provides a PPF that can adjust adaptively if the tracking error violation occurs. It can ensure that the tracking error no longer violates the constraint through adaptive expansion.

In addition, the PPF structural parameters ρ_0 is set according to the initial error size, l, ψ_1 and ψ_2 are the constant parameters we can design. It can make the PPF structural parameters to be set more flexible.

Besides, a periodic scaling scheme is adopted. It can avoid the buffeting effect of the control response caused by frequent PPF scaling. According to the above scheme, the adaptive scaling PPF can be realised.

https://doi.org/10.1017/aer.2023.79 Published online by Cambridge University Press

We summarise the implementation of adaptive scaling strategy in Algorithm 1.

Algorithm 1 The implementation of adaptive scaling strategy.

Initialisation:

1. Initialise the scaling coefficient $k = \bar{k} = 1$, the flag variable $F_1 = F_2 = 0$. Set $\rho_0 = l \cdot |e_0| + \psi_1$, $\rho_\infty = \psi_2$.
2. Initialise the states parameters.
3. Calculate the initial PPF.

Iteration:

Step 1. Judge whether $-L\rho(t) < e(t) < U\rho(t)$. If satisfied, $F_1 = 0$, else $F_1 = 1$.

Step 2. if $(F_1 == 0)$ & & $(F_2 == 0)$
then $k = 1$; $\bar{k} = 1$; goto **Step 6**;
else if $(F_1 == 0)$ & & $(F_2 == 1)$
then $\bar{k} = 1$; goto **Step 6**;
else if $F_1 == 1$
then goto **Step 3**;
end.

Step 3. If $|\dot{e}(t)| \leq \tan(\vartheta)$
then $k = \left(1 + \tanh\left(\frac{|e(t)|}{h}\right)\right) \cdot \bar{k}$; $\bar{k} = k$;
else if $|\dot{e}(t)| > \tan(\vartheta)$
then $k = \left(1 + |\dot{e}(t)| \cdot \tanh\left(\frac{|e(t)|}{h}\right)\right) \cdot \bar{k}$; $\bar{k} = k$;
end

Step 4. Repeat **Step 1**.
If $F_1 == 0$
then goto **Step 5**;
else if $F_1 == 1$
then goto **Step 3**;
end

Step 5. Update the PPF and lock the scaling coefficient k for time T. During the period of T, set the $F_2 = 1$.

Step 6. Update the unconstrained error $\varepsilon(t)$, the control and flight states.

Substituting the coefficients k, ρ_0 and ρ_∞ of Algorithm 1 into the Equations (13–18), then we can get the new ε, T_d and T_c. Therefore, according to the PPC principle, as long as we design the controller to ensure that the virtual error ε is bounded, the tracking error of the original system will satisfy the constraint performance $-L\rho(t) \leq e_i(t) \leq U\rho(t)$ we designed.

Remark 1. *The Algorithm 1 includes the PPF of expanding and resuming. If the signal of the tracking error violation occurs, the PPF is adaptively expanded according to the angle error and angle error change rate, where h is the sensitivity coefficient. ϑ represents the error trend angle of the scaling point, while $\tan(\vartheta)$ corresponds to the error derivative of the scaling point. By adjusting the appropriate ϑ, we can obtain two types of scaling. We hope that the expanded PPF can reasonably cover the error changes. Expansion methods based on error and error change rate are more predictive and reasonable. Too frequent or excessive expansion is detrimental to the tracking performance of the system. Compared to arbitrary expansion methods, this scheme can ensure the use of reasonable expansion times and degrees. Based on the angle error and angle error change rate, we can design two expansion schemes with different degrees of conservatism. It will guarantee as proper times and degrees of expansion as possible.*

https://doi.org/10.1017/aer.2023.79 Published online by Cambridge University Press

Remark 2. *The expansion in algorithm1 has high priority. As long as the tracking error violation occurs at any time, the expansion in the Algorithm 1 will be triggered and the expansion coefficient will be locked. Once triggered, the scaling coefficient will be locked and maintained for time T. At the end of the time T, the algorithm can recover to normal PPF ($k = 1$) immediately after judging no violation. If the tracking error still violates the constraint after expanding, it can still expand according to the previous expansion until no violation, and so on. The setting of T ensures the buffer effect of PPF's expansion after the violation.*

Remark 3. *PPF structure parameter ρ_0 is set to $\rho_0 = l \cdot |e_0| + \psi_1$. In this way, it is associated with the initial error and become more flexible. By adding a set of smaller constants ψ_1 and ψ_2 as constraints, it can avoid PPF being too tight and causing frequent state violation.*

3.2 Disturbance observer

Considering the uncertainties and disturbances in Equation (12), the controller own robustness cannot effectively resist the disturbance. So a nonlinear disturbance observer (NDO) is adopted to observe and compensate the disturbance [29], making the system more robust.

Lemma 1. [29] *Consider the following system:*

$$\begin{aligned} \dot{x}_1 &= x_2 \\ \dot{x}_2 &= F(x_1, x_2) \end{aligned} \tag{19}$$

where $x_1, x_2 \in R^{1\times 1}$. If system (19) satisfies the conditions of $x_1(t) \to 0, x_2(t) \to 0 (t \to \infty)$, then for any arbitrary continuous bounded function $v(t)$, $T > 0$ and $Q > 0$, the solution of the following system:

$$\begin{aligned} \dot{x}_1 &= x_2 \\ \dot{x}_2 &= Q^2 F\left(x_1 - v(t)\,, \frac{x_2}{Q}\right) \end{aligned} \tag{20}$$

satisfies:

$$\lim_{Q\to\infty} \int_0^T |x_1 - v(t)|\, dt = 0 \tag{21}$$

Lemma 1 indicates that if Q is selected to be sufficient large, then x_1 averagely converges to the input signal $v(t)$ and x_2 weakly converges to the generalised differentiation of $\dot{v}(t)$.

Theorem 1. *Consider the following system:*

$$\begin{aligned} \dot{x}_1 &= x_2 \\ \dot{x}_2 &= Q^2 \left(-h_1 \tanh(x_1) - h_2 \tanh\left(\frac{x_2}{Q}\right)\right) \end{aligned} \tag{22}$$

where, $x_1, x_2, h_1, h_2, Q \in R^{1\times 1}$. Define the candidate Lyapunov function as follows:

$$V_1 = \int_0^{x_1} Q^2 h_1 \tanh(\xi)\, d\xi + \frac{1}{2} x_2^2 \tag{23}$$

The derivative of Equation (23) *can be obtained,*

$$\begin{aligned} \dot{V}_1 &= h_1 Q^2 \tanh(x_1)\, x_2 + x_2 \dot{x}_2 \\ &= -h_2 Q^2 \tanh\left(\frac{x_2}{Q}\right) x_2 \\ &\le 0 \end{aligned} \tag{24}$$

https://doi.org/10.1017/aer.2023.79 Published online by Cambridge University Press

Therefore, when $h_1, h_2 > 0$, the system is asymptotically stable at $(0, 0)$. The $F(x_1, x_2)$ we selected satisfies the Lemma 1.

Now, consider the system as follows :

$$\dot{z} = f(z) + g(z)\, u + d \tag{25}$$

where, $z \in R^{n\times 1}$ is the state, $f(z) \in R^{n\times 1}$ and $g(z) \in R^{n\times n}$ are continuous functions, $u \in R^{n\times 1}$ is the control quantity, $d \in R^{n\times 1}$ is the sum of unmodeled dynamics and disturbances.

Theorem 2. [29] *Consider the following system:*

$$\begin{aligned} \dot{\hat{z}} &= f(z) + g(z)\, u + \hat{d} \\ \dot{\hat{d}} &= Q^2 \left(-h_1 \tanh\left(\hat{z} - z\right) - h_2 \tanh\left(\frac{\hat{d}}{Q}\right) \right) \end{aligned} \tag{26}$$

where, $\hat{z}$ and $\hat{d}$ are the estimates of z and d. $h_1, h_2, Q \in R^{1\times 1}$ represent adjustable observer parameters. If $T > 0$ and $Q > 0$, the

$$\lim_{Q\to\infty} \int_0^T \left|\hat{z} - z\right| dt = 0 \tag{27}$$

holds true, it means that $\hat{z}$ approaches z. Furthermore, based on Equations (25 and 26), we can obtain that $\hat{d} \to d$.

According to Theorem 1 and Lemma 1, it can be seen that the value of $\left|\dot{\hat{d}}\right| = \left|Q^2 F\left(\hat{z} - z, \frac{\hat{d}}{Q}\right)\right|$ may be infinitely large when $Q \to \infty$. It denotes that $\hat{d}$ varies much faster than $f(z) + g(z)\, u$. Then we have

$$\lim_{Q\to\infty} \frac{d\left(f(z) + g(z)\, u + \hat{d}\right)}{dt} \approx \dot{\hat{d}} \tag{28}$$

$$\lim_{Q\to\infty} \frac{f(z) + g(z)\, u + \hat{d}}{Q} \approx \frac{\hat{d}}{Q} \tag{29}$$

Then, replacing x_2 in Equation (20) by $f(z) + g(z)\, u + \hat{d}$, the Equations (26 and 27) always hold true.

Assumption 4. [30] *The d and $\dot{d}$ are bounded. Based on this assumption, the system disturbance could be observed. Thus all of the continuous and bounded system disturbances satisfy this assumption. The stability analysis of disturbance estimation is feasible.*

Remark 4. [31] *Although only when $Q \to \infty$ one can get $\hat{d} \to d$ in theory. Simulation studies show that an effective estimation performance can be also obtained using the proposed NDO (26) by choosing a finite Q. $\hat{d} \to d$ can still converge to a small convergence domain.*

Remark 5. *The parameter analysis of the NDO is as follows: Q, h_1 and h_2 are related to the convergence speed and convergence accuracy. Increasing Q or h_1 will improve the convergence speed and convergence accuracy, but an excessively large Q or h_1 will increase the high-frequency oscillation during convergence process; h_2 has the opposite effect. Increasing h_2 is beneficial for suppressing high frequency oscillation, but excessive h_2 can slow down convergence speed and reduce accuracy. The parameter tuning process is as follows: First, select a large Q as the dominant factor. Second, select a small h_1 to continue to fine-tune the system. Last, select a small h_2 to suppress the high frequency oscillation during convergence process. We provide the effectiveness verification of NDO in section 4.*

https://doi.org/10.1017/aer.2023.79 Published online by Cambridge University Press

According to the above analysis, combing the nonlinear model (12), we can write the disturbance observer model in the form of (30–31) :

$$\begin{aligned}\dot{\hat{\theta}} &= g_s\omega + \hat{\Delta}_s \\ \dot{\hat{\Delta}}_s &= {R_s}^2\left(-h_{s1}\tanh\left(\hat{\theta}-\theta\right) - h_{s2}\tanh\left(\frac{\hat{\Delta}_s}{R_s}\right)\right)\end{aligned} \tag{30}$$

$$\begin{aligned}\dot{\hat{\omega}} &= g_f U + f_f(\omega) + \hat{\Delta}_f \\ \dot{\hat{\Delta}}_f &= {R_f}^2\left(-h_{f1}\tanh\left(\hat{\omega}-\omega\right) - h_{f2}\tanh\left(\frac{\hat{\Delta}_f}{R_f}\right)\right)\end{aligned} \tag{31}$$

where, $\hat{\theta}$, $\hat{\omega}$, $\hat{\Delta}_s$, $\hat{\Delta}_f$ are the estimated values of θ, ω, Δ_s, Δ_f. In addition, we define $\tilde{\theta} = \hat{\theta} - \theta$, $\tilde{\omega} = \hat{\omega} - \omega$, $\tilde{\Delta}_s = \hat{\Delta}_s - \Delta_s$, $\tilde{\Delta}_f = \hat{\Delta}_f - \Delta_f$ as the corresponding estimation errors of NDO. By designing and adjusting the appropriate parameter R_s, h_{s1}, h_{s2}, R_f, h_{f1}, h_{f2}, we can ensure that the estimation errors satisfy $\|\tilde{\theta}\| < \bar{\theta}$, $\|\tilde{\omega}\| < \bar{\omega}$, $\|\tilde{\Delta}_s\| < \bar{\Delta}_s$, $\|\tilde{\Delta}_f\| < \bar{\Delta}_f$. $\bar{\theta}$, $\bar{\omega}$, $\bar{\Delta}_s$ and $\bar{\Delta}_f$ are their upper bounds.

3.3 Design of prescribed performance dynamic surface controller

Step 1: Define the first dynamic surface $S_1 = \varepsilon$ and error $e_1 = \theta - \theta_d$. $\theta_d \in R^{3\times 1}$ is the given command angle. Combined with the Equations (16–18), we can get the derivative of S_1 as follows:

$$\begin{aligned}\dot{e}_1 &= g_s\omega + \Delta_s - \dot{\theta}_d \\ \dot{S}_1 &= T_d\dot{e}_1 + T_c\end{aligned} \tag{32}$$

According to method of dynamic surface controller, the virtual control law ω_1 is proposed as:

$$\omega_1 = {g_s}^{-1}\left(\dot{\theta}_d - \hat{\Delta}_s - {T_d}^{-1}T_c - C_1S_1\right) \tag{33}$$

where, $C_1 = diag(C_{11}, C_{12}, C_{13})$. C_{11}, C_{12}, C_{13} are positive constants.

Next, in order to avoid the complexity, let ω_1 pass through a first-order filter with time constant τ, given by:

$$\tau\dot{\omega}_d + \omega_d = \omega_1, \omega_d(0) = \omega_1(0) \tag{34}$$

Within this setting, $\dot{\omega}_d$ can be calculated by $\dfrac{(\omega_1 - \omega_d)}{\tau}$ without direct differential operation of ω_d. Further, the error of the low filter is defined as:

$$\sigma = \omega_d - \omega_1 \tag{35}$$

Step 2: Define the second dynamic surface $S_2 = \omega - \omega_d$. Taking the derivative of S_2 with respect to time yields:

$$\dot{S}_2 = \dot{\omega} - \dot{\omega}_d \tag{36}$$

Consider the candidate Lyapunov function as :

$$V_2 = \frac{1}{2}{S_1}^T S_1 + \frac{1}{2}{S_2}^T S_2 + \frac{1}{2}\sigma^T\sigma \tag{37}$$

https://doi.org/10.1017/aer.2023.79 Published online by Cambridge University Press

The derivative of V_2 can be written as :

$$\begin{aligned}\dot{V}_2 &= {S_1}^T \dot{S}_1 + {S_2}^T \dot{S}_2 + \sigma^T \dot{\sigma} \\ &= {S_1}^T \left(T_d \dot{e}_1 + T_c\right) + {S_2}^T \left(g_f U + f_f\left(\omega\right) + \Delta_f - \dot{\omega}_d\right) + \sigma^T \dot{\sigma} \\ &= {S_1}^T \left(T_d \left(g_s \sigma + g_s S_2 + g_s \omega_1 + \Delta_s - \dot{\theta}_d\right) + T_c\right) \\ &\quad + {S_2}^T \left(g_f U + f_f\left(\omega\right) + \Delta_f - \dot{\omega}_d\right) + \sigma^T \dot{\sigma} \\ &= {S_1}^T \left(T_d \left(-\tilde{\Delta}_s + g_s S_2 + g_s \sigma - C_1 S_1\right)\right) \\ &\quad + {S_2}^T \left(g_f U + f_f\left(\omega\right) + \Delta_f - \dot{\omega}_d\right) + \sigma^T \dot{\sigma} \\ &= -\left(T_d S_1\right)^T \tilde{\Delta}_s + {S_1}^T \left(T_d g_s S_2\right) + {S_1}^T \left(T_d g_s \sigma\right) \\ &\quad - {S_1}^T \left(T_d C_1\right) S_1 + {S_2}^T \left(g_f U + f_f\left(\omega\right) + \Delta_f - \dot{\omega}_d\right) + \sigma^T \dot{\sigma}\end{aligned} \tag{38}$$

To stabilise V_2, the control law U is proposed as:

$$U = {g_f}^{-1} \left(-f_f - \hat{\Delta}_f + \dot{\omega}_d - T_d g_s S_1 - C_2 S_2 - \frac{{S_1}^T \left(T_d g_s \sigma\right) S_2}{\left\|S_2\right\|^2} - T_d {g_s}^T S_1\right) \tag{39}$$

where, $C_2 = diag(C_{21}, C_{22}, C_{23})$. C_{21}, C_{22}, C_{23} are positive constants.

Combining the disturbance observer form designed by Equations (30 and 31) and substituting the Equations (33) and (39) into Equation (38), we can get :

$$\begin{aligned}\dot{V}_2 &= -\left(T_d S_1\right)^T \tilde{\Delta}_s + {S_1}^T \left(T_d g_s \sigma\right) - {S_1}^T \left(T_d C_1\right) S_1 \\ &\quad - {S_2}^T \tilde{\Delta}_f - {S_2}^T C_2 S_2 + \sigma^T \dot{\sigma}\end{aligned} \tag{40}$$

According to the well-known Young's inequality [32], we can obtain the following inequality:

$$-\left(T_d S_1\right)^T \tilde{\Delta}_s \leq \frac{\chi_1}{2} \left(T_d S_1\right)^T \left(T_d S_1\right) + \frac{1}{2\chi_1} \tilde{\Delta}_s^T \tilde{\Delta}_s \tag{41}$$

$$-{S_2}^T \tilde{\Delta}_f \leq \frac{\chi_2}{2} {S_2}^T S_2 + \frac{1}{2\chi_2} \tilde{\Delta}_f^T \tilde{\Delta}_f \tag{42}$$

where χ_1 and χ_2 is a positive tuning parameter. Then, we have

$$\begin{aligned}\dot{V}_2 &\leq \frac{\chi_1}{2} \left(T_d S_1\right)^T \left(T_d S_1\right) + \frac{1}{2\chi_1} \tilde{\Delta}_s^T \tilde{\Delta}_s + \frac{\chi_1}{2} {S_2}^T S_2 \\ &\quad + \frac{1}{2\chi_1} \tilde{\Delta}_f^T \tilde{\Delta}_f - {S_1}^T \left(T_d C_1\right) S_1 - {S_2}^T C_2 S_2 + \sigma^T \dot{\sigma}\end{aligned} \tag{43}$$

Integrating the Equations (34 and 35), we have

$$\begin{aligned}\sigma^T \dot{\sigma} &= \sigma^T \left(-\frac{\sigma}{\tau} - \dot{\omega}_1\right) \\ &= -\frac{1}{\tau} \sigma^T \sigma - \sigma^T \dot{\omega}_1\end{aligned} \tag{44}$$

Lemma 2. [33] *The virtual control law ω_1 is bounded and satisfies: $\|\dot{\omega}_1\| \leq \eta$, η is a nonnegative continuous function.*

https://doi.org/10.1017/aer.2023.79 Published online by Cambridge University Press

Therefore, according to the Lemma 2 and Young's inequality, we can obtain the following inequality:

$$\begin{aligned}\sigma^T\dot{\sigma} &= -\frac{1}{\tau}\sigma^T\sigma - \sigma^T\dot{\omega}_1 \\ &\le -\frac{1}{\tau}\sigma^T\sigma + \frac{\chi_3}{2}\sigma^T\sigma + \frac{1}{2\chi_3}\dot{\omega}_1^T\dot{\omega}_1 \\ &\le \left(\frac{\chi_3}{2} - \frac{1}{\tau}\right)\sigma^T\sigma + \frac{\eta^2}{2\chi_3}\end{aligned} \tag{45}$$

where χ_3 is a positive tuning parameter.

Integrating the Equations (43) and (45), $\dot{V}_2$ satisfies the following inequality :

$$\begin{aligned}\dot{V}_2 &\le \frac{\chi_1}{2}(T_dS_1)^T(T_dS_1) + \frac{1}{2\chi_1}\tilde{\Delta}_s^T\tilde{\Delta}_s - S_1{}^T(T_dC_1)S_1 + \frac{\chi_2}{2}S_2{}^TS_2 \\ &\quad + \frac{1}{2\chi_2}\tilde{\Delta}_f^T\tilde{\Delta}_f - S_2{}^TC_2S_2 + \left(\frac{\chi_3}{2} - \frac{1}{\tau}\right)\sigma^T\sigma + \frac{\eta^2}{2\chi_3} \\ &= -S_1{}^T\left[T_d\left(C_1 - \frac{\chi_1}{2}T_d\right)\right]S_1 + \frac{1}{2\chi_1}\|\tilde{\Delta}_s\|^2 - S_2^T\left(C_2 - \frac{\chi_2}{2}\cdot I_{3\times3}\right)S_2 \\ &\quad + \frac{1}{2\chi_2}\|\tilde{\Delta}_f\|^2 - \left(\frac{1}{\tau} - \frac{\chi_3}{2}\right)\sigma^T\sigma + \frac{\eta^2}{2\chi_3}\end{aligned} \tag{46}$$

Let $M_1 = \frac{1}{2\chi_1}\|\tilde{\Delta}_s\|^2$, $M_2 = \frac{1}{2\chi_2}\|\tilde{\Delta}_f\|^2$, $M_3 = \frac{\eta^2}{2\chi_3}$. They are satisfied:

$$\begin{aligned}M_1 &< \frac{1}{2\chi_1}\bar{\Delta}_s^2 \\ M_2 &< \frac{1}{2\chi_2}\bar{\Delta}_f^2\end{aligned} \tag{47}$$

Consider $\Omega = \left\{\left(S_1, S_2, \sigma, \tilde{\Delta}_s, \tilde{\Delta}_f\right) : V_2 \le p\right\}$ is a compact set. Thereby, η has a maximum value $\bar{\eta}$ on Ω. let $M = \frac{1}{2\chi_1}\bar{\Delta}_s^2 + \frac{1}{2\chi_2}\bar{\Delta}_f^2 + \frac{\bar{\eta}^2}{2\chi_3}$, which leads to

$$\begin{aligned}\dot{V}_2 &\le -S_1{}^T\left[T_d\left(C_1 - \frac{\chi_1}{2}T_d\right)\right]S_1 + M_1 - S_2^T\left(C_2 - \frac{\chi_2}{2}\cdot I_{3\times3}\right)S_2 + M_2 - \left(\frac{1}{\tau} - \frac{\chi_3}{2}\right)\sigma^T\sigma + M_3 \\ &\le -S_1{}^T\left[T_d\left(C_1 - \frac{\chi_1}{2}T_d\right)\right]S_1 - S_2^T\left(C_2 - \frac{\chi_2}{2}\cdot I_{3\times3}\right)S_2 - \left(\frac{1}{\tau} - \frac{\chi_3}{2}\right)\sigma^T\sigma + M\end{aligned} \tag{48}$$

Lemma 3. [32] *$\zeta_{min}X^TX \le X^TAX \le \zeta_{max}X^TX$, $A \in R^{n\times n}$ is a real symmetric matrix. ζ_{min} and ζ_{max} are the minimum and maximum eigenvalues of matrix A. $X \in R^{n\times1}$ is the arbitrary matrix.*

According to the Lemma 3, by choosing appropriate parameters c_1, c_2, τ, χ_1, χ_2, χ_3 and define $A = \left(T_dC_1 - \frac{\chi_1}{2}T_d{}^TT_d\right)$, $B = \left(C_2 - \frac{\chi_2}{2}\cdot I_{3\times3}\right)$, $C = \left(\frac{1}{\tau} - \frac{\chi_3}{2}\right)$ as real symmetric matrixs. Then $\dot{V}_2$ is satisfied:

$$\begin{aligned}\dot{V}_2 &\le -\zeta_1S_1{}^TS_1 - \zeta_2S_2{}^TS_2 - \zeta_3\sigma^T\sigma + M \\ &\le -\zeta S_1{}^TS_1 - \zeta S_2{}^TS_2 - \zeta\sigma^T\sigma + M \\ &\le -2\zeta V_2 + M\end{aligned} \tag{49}$$

where, ζ_1, ζ_2, ζ_3 are the positive minimum eigenvalues of the real symmetric matrixs A, B, C. $\zeta = \min\{\zeta_1, \zeta_2, \zeta_3\}$.

https://doi.org/10.1017/aer.2023.79 Published online by Cambridge University Press

Table 1. *HV and environment parameters*

Variables	Symbols	Value
Mass	m	63,500 kg
Reference aerodynamic chord	c	24.38m
Wing span	b	18.29m
Reference area	S	334.73m^2
x-axis moment of inertia	J_x	637,234 $kg \cdot m^2$
y-axis moment of inertia	J_y	6,101,181 $kg \cdot m^2$
z-axis moment of inertia	J_z	6,101,181 $kg \cdot m^2$
The distance from the pressure centre to the mass centre	x_{cg}	4.467m
Acceleration of gravity coefficient	g_0	9.8m/s^2
Earth radius at the poles	R_e	6356.766km
Atmospheric density coefficient	ρ_0	1.226kg/m^3
Equivalent atmospheric scale height	H_0	7315.2m
Flight path angle	γ	0 rad
Flight velocity	V	4,590 m/s
Flight altitude (Distance from sea level)	H	33km

By comparison principle, it is easy from Equation (49) to obtain that

$$V_2 \leq \frac{M}{2\zeta} + \left(V_2(0) - \frac{M}{2\zeta} \right) e^{-2\zeta t} \tag{50}$$

According to (50), if $2\zeta \geq \frac{M}{p}$, then we have $\dot{V}_2 \leq 0$ and $V_2 \leq p$ is an invariant set. Therefore, if $V_2(0) \leq p$, then $V_2(t) \leq p$, for all $t > 0$. In addition, S_1, S_2, σ are all semi-globally uniformly ultimately bounded. By choosing proper ζ, and the convergence bound can be set as small as possible. Furthermore, the unconstrained error is bounded. According to the previous conclusion, e_1 can also meet the prescribed performance requirements.

4.0 Numerical simulations

This section will use the control laws in Equations (33 and 34) and (39), disturbance estimations Equations (30 and 31) for simulation verification and analysis. The simulation verification of the command tracking with continuous time-varying external disturbances and other uncertain parameters are implemented.

The parameters of HV model in this paper are shown in Table 1.

The parameters of controller and disturbance observer in this paper are shown in Table 2.

The parameters related to the adaptive scaling strategy are shown in Table 3.

The HV uncertainty model and the time-varying external disturbances (apply within 20s–30s) are shown in Table 4.

We take the attitude control problem of HV longitudinal channel as an example. We focus on the angle-of-attack simulation results. The 6-degree of freedom simulations are implemented. The command angle of sideslip and command angle of bank are set to fixed 0 (rad). In the simulation, we set the initial angle $\theta = [0.14, 0, 0]^T$ (rad), initial angle velocity $\omega = [0, 0, 0]^T$ (rad/s). Besides, considering the limit of the elevons, we set $|\delta| \leq 20^\circ$.

Due to the inability to provide explicit forms of system disturbances in the model of HV. Therefore, it is difficult to provide a comparison chart between the disturbance terms and NDO observation results. So the observation effect of NDO on system disturbances is verified here through the simple system shown as Equation (25). The specific form is shown in Equation (51). The disturbance estimation method is

https://doi.org/10.1017/aer.2023.79 Published online by Cambridge University Press

Table 2. *Controller and disturbance observer parameters*

Components	Numerical value
Outer loop control law	$C_1 = diag(2, 2, 2)$
Outer loop disturbance observer	$R_s = 60$, $h_{s1} = 1$, $h_{s2} = 0.8$
Inner loop control law	$C_2 = diag(1, 1, 1)$, $\tau = 0.005$
Inner loop disturbance observer	$R_f = 60$, $h_{f1} = 1$, $h_{f2} = 0.8$

Table 3. *Relevant parameters of adaptive scaling strategy*

Components	Numerical value
Relevant parameters of adaptive scaling strategy	$L = U = 1$, $\lambda = 0.1$, $l = 1.1$, $\psi_1 = 1$, $\psi_2 = 0.8$, $T = 2$, $h = 6$, $\vartheta = \frac{\pi}{2}$

Table 4. *Uncertainty and disturbances parameters*

Components	Numerical value
ΔC_L	10%
ΔC_m	10%
$\Delta\bar{q}$(Dynamic pressure)	10%
d_α, d_q (Small disturbance)	$0.01sin\,(0.5t) + 0.01sin\,(t) + 0.01sin\,(1.5t) + 0.01sin\,(2t)$
d_α, d_q (Large disturbance)	$0.1sin\,(0.5t) + 0.1sin\,(t) + 0.1sin\,(1.5t) + 0.1sin\,(2t)$

shown as Equation (26). The selected NDO parameters are also shown as $Q = 60$, $h_1 = 1$, $h_2 = 0.8$.

$$\begin{aligned} \dot{z} &= f(z) + g(z)\,U + d \\ z_d &= \sin(t) \\ U &= g^{-1}(z)\left[-10(z - z_d) - f(z) - \hat{d} + \dot{z}_d\right] \\ f(z) &= z^2 + z + 2\sin(z) + 1 \\ g(z) &= 10 \end{aligned} \tag{51}$$

where, the given test disturbance is set to $0.1sin(0.5t) + 0.1sin\,(t) + 0.1sin\,(1.5t) + 0.1sin\,(2t)$. Figure 4(a–d) show the relevant test results of NDO.

Comparing with the dynamic surface control method under observer compensation (DSC-NDO, the green line in Figs. 5(b) and 6(b)) and the prescribed performance sliding mode control method (PPSMC, the red line in Figs. 5(b) and 6(b)) to verify the advantages of the proposed method (IPPDSC-NDO, the blue line in Figs. 5(b) and 6(b), the black line in Fig. 7). To prove the effectiveness of adaptive scaling

https://doi.org/10.1017/aer.2023.79 Published online by Cambridge University Press

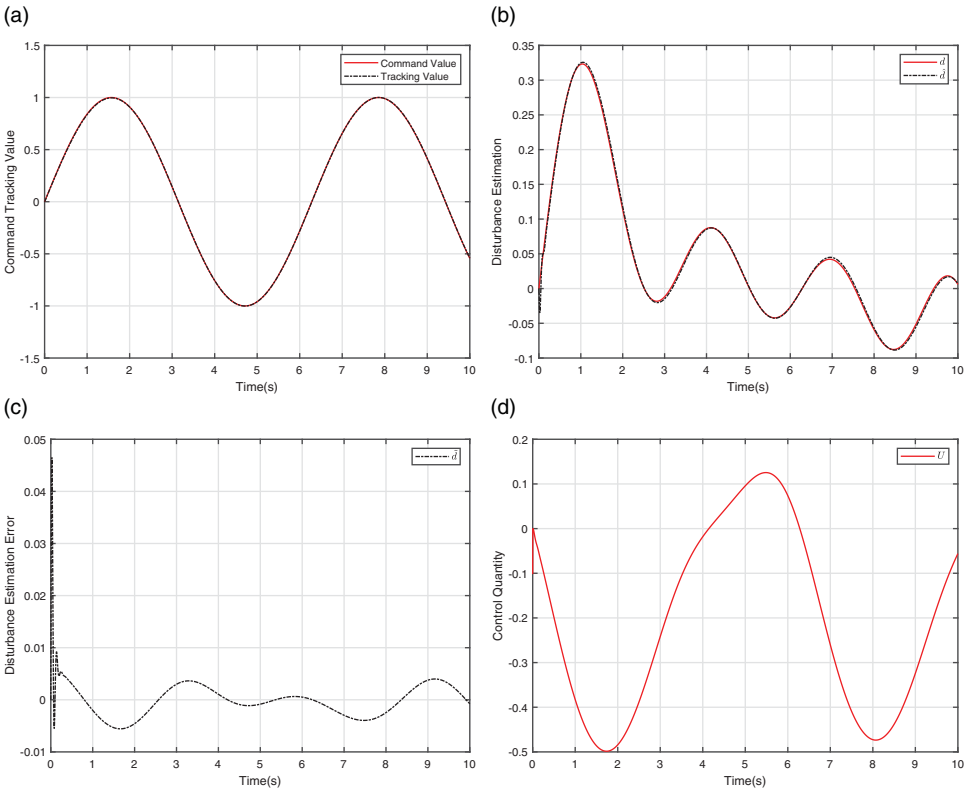

Figure 4. *Simulation results of the NDO.*

strategy, the method in this paper is also compared with the scheme without applying the adaptive scaling strategy (PPDSC-NDO, the red line in Fig. 7).

4.1 Simulation results of the NDO

Figure 4(b, c) show the estimation effect of the NDO on disturbance. The disturbance estimation error is shown in Fig. 4(c), and it is bounded. The tracking effect of the given is shown in Fig. 4(a). Figure 4(d) shows the control quantity. Therefore, the NDO can be used to estimate the disturbance of the attitude control system.

4.2 Simulation results with uncertainties and small external disturbances

Figure 5(a, b) show that the proposed method has better control effect than other method under small external disturbances and uncertainties. Figure 5(c–e) show the other states simulation results of the proposed method. The elevons are shown in Fig. 5(c). The disturbance estimations are shown in Fig. 5(d). The virtual error of the angle-of-attack is shown in Fig. 5(e), and it is bounded.

Compared with the DSC-NDO and PPSMC, it has smaller overshoot and better transient response. Besides, it has no buffeting effect.

4.3 Simulation results with uncertainties and large external disturbances

Figure 6(a, b) show that the proposed method still has better control effect than other methods under large external disturbances and uncertainties. Figure 6(c–f) show the other states simulation results of

https://doi.org/10.1017/aer.2023.79 Published online by Cambridge University Press

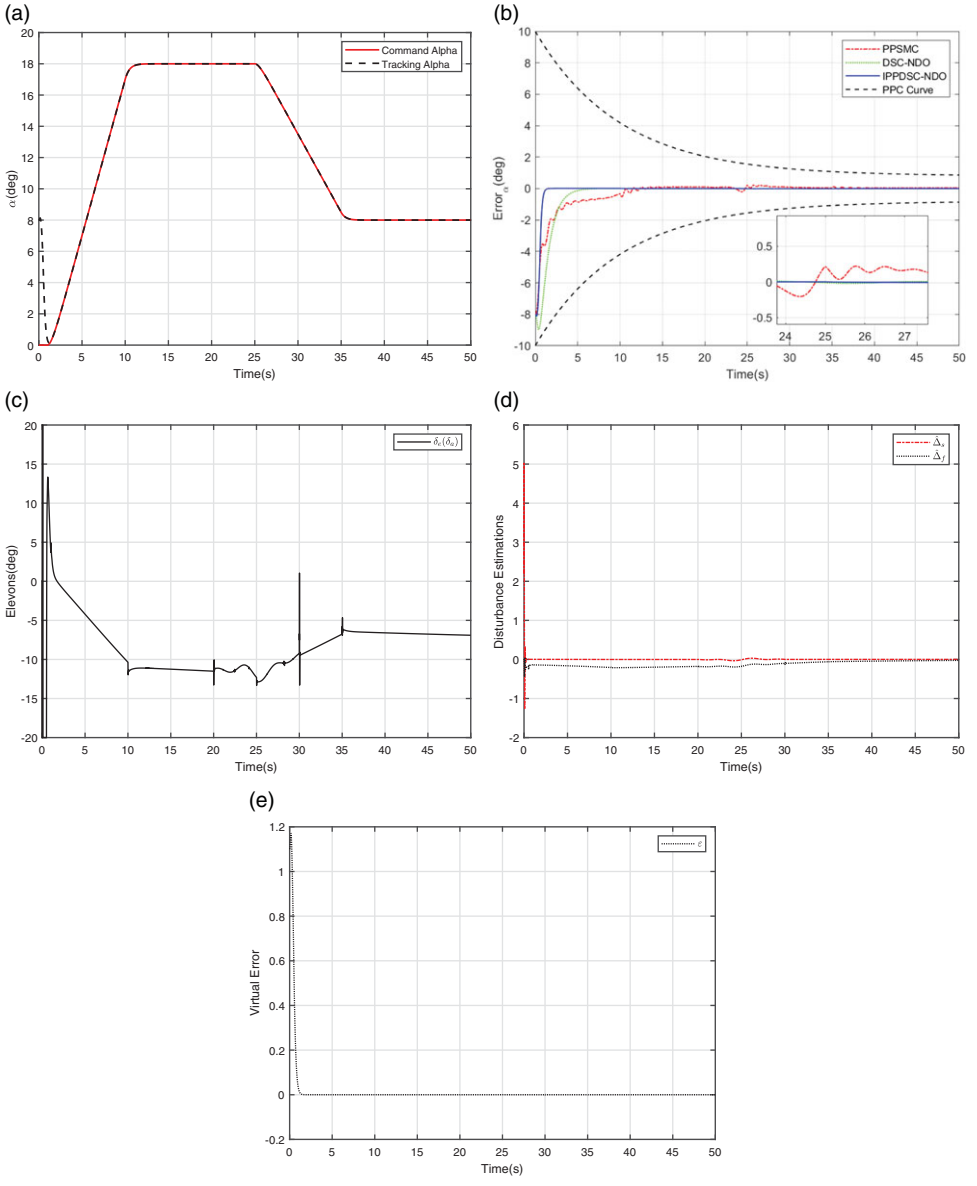

Figure 5. *Simulation results with uncertainties and small external disturbances.*

the proposed method. The elevons of the proposed method are shown in Fig. 6(c). The disturbance estimations are shown in Fig. 6(d). The virtual error of the angle-of-attack is shown in Fig. 6(e), and it is also bounded. The change of the scaling coefficient is shown in Fig. 6(f).

It can be seen from the Fig. 6(b) that the PPSMC has diverged and cannot complete the stability control of the system. Although the dynamic surface control method with observer compensation has achieved stable control, its overshoot and transient response are significantly weaker than the control method proposed in this paper. Besides, it can be seen that the system expanded the PPF at 25.86s, 26.24s and returned to normal at 28.24s, verifying the high priority of the Algorithm 1. Under this method, we can see that the error (blue line) doesn't violate the constraint with a proper expansion. The extent of expansion is also reasonable. Therefore, compared with other methods, the control method proposed in this paper can not only ensure excellent dynamic performance, but also have strong robustness.

https://doi.org/10.1017/aer.2023.79 Published online by Cambridge University Press

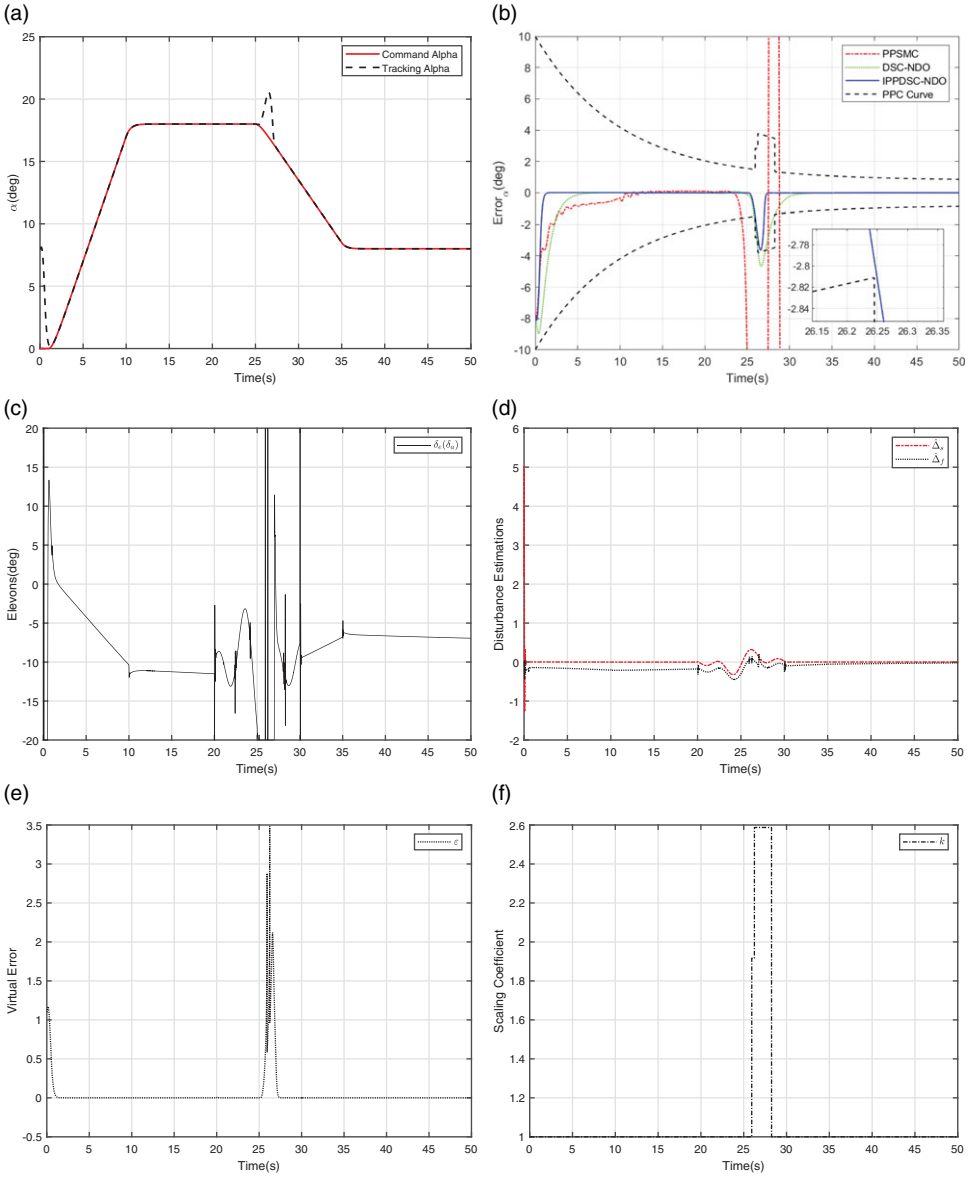

Figure 6. *Simulation results with uncertainties and large external disturbances.*

4.4 Simulation results with and without adaptive scaling strategy under uncertainties and large external disturbances

Under large external disturbances and uncertainties, the strategy proposed in this paper plays an important role in Fig. 7. It can ensure the stability of the system by adaptively adjusting the constraint of PPF, while the non-strategy control appears divergent phenomenon. Therefore, it further verifies the effectiveness of the control method and the adaptive scaling strategy proposed in this paper.

This paper mainly investigates the constrained attitude control problem of HVs under large disturbances and uncertainties. Although the method proposed in this paper takes the attitude control of HV as an example, we believe that it can also be used in other fields; for example, the control problem of near-space vehicle and the industrial control problem of complex working conditions. The research

https://doi.org/10.1017/aer.2023.79 Published online by Cambridge University Press

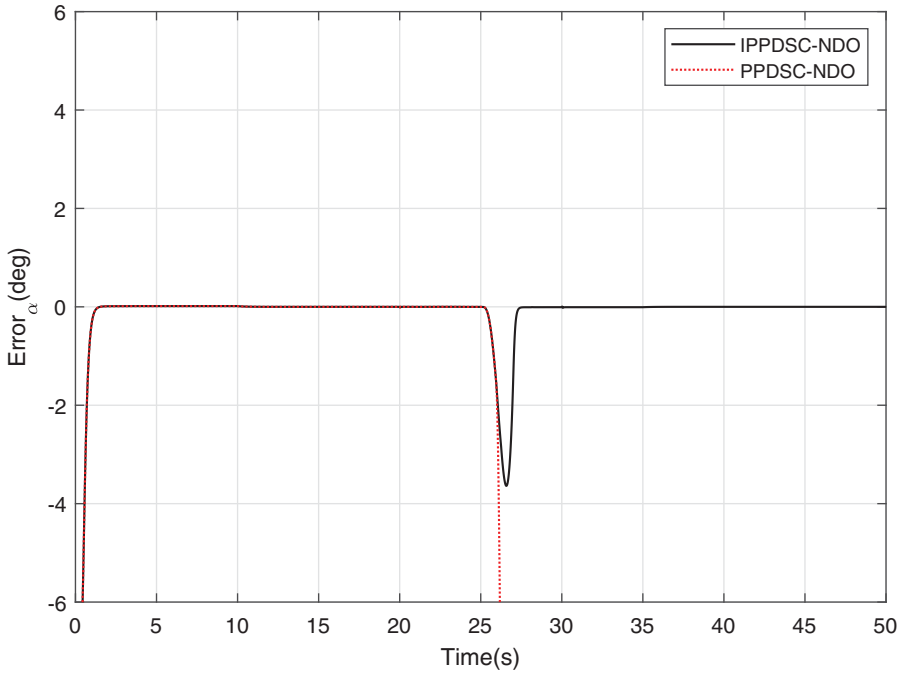

Figure 7. *Simulation results with and without adaptive scaling strategy under uncertainties and large external disturbances.*

background of these issues often has strong uncertainties and disturbances, which is consistent with the research background of this paper. We hope this method can have a certain promotional effect.

5.0 Conclusion

This paper proposes an improved prescribed performance dynamic surface control method with an adaptive scaling strategy. This method achieves good tracking control of the HV attitude command angle. Compared with the traditional PPF, the PPF designed in this paper can scale adaptively according to the relevant state and avoid the tracking error violation. In addition, a NDO is introduced to enhance the robustness of the system. Thus, based on the PPC framework and NDO, it improves both robustness and dynamic performance of the system. Finally, the numerical simulation results verify the effectiveness of the control method we design.

Acknowledgments. The authors would like to express their sincere gratitude for the support of the National Natural Science Foundation of China (Grant/Award Numbers: 61873319).

References

[1] Xu B. and Shi Z.K. An overview on flight dynamics and control approaches for hypersonic vehicles. *Sci. China Inf. Sci.*, 2015, **58**, (7), pp 1–19.
[2] Ding Y.B., Yue X.K., Chen G.S. and Si J.S. Review of control and guidance technology on hypersonic vehicle. *Chin. J. Aeronaut.*, 2022, **35**, (7), pp 1–18.
[3] Sun H.B., Li S.H., Yang J. and Guo L. Non-linear disturbance observer-based back-stepping control for airbreathing hypersonic vehicles with mismatched disturbances. *Chin. J. Aeronaut.*, 2014, **8**, (17), pp 1852–1865.
[4] An H., Liu J.X., Wang C.H. and Wu L.G. Approximate back-stepping fault-tolerant control of the flexible air-breathing hypersonic vehicle. *IEEE/ASME Trans. Mechatron.*, 2015, **21**, (3), pp 1680–1691.
[5] Zong Q., Wang F., Tian B.L. and Su R. Robust adaptive dynamic surface control design for a flexible air-breathing hypersonic vehicle with input constraints and uncertainty. *Nonlinear Dyn.*, 2014, **78**, pp 289–315.

https://doi.org/10.1017/aer.2023.79 Published online by Cambridge University Press

[6] Sagliano M., Mooij E. and Theil S. Adaptive disturbance-based high-order sliding-mode control for hypersonic-entry vehicles. *J. Guid. Control Dyn.*, 2017, **40**, (3), pp 521–536.
[7] Sun H.B., Li S.H. and Sun C.Y. Finite time integral sliding mode control of hypersonic vehicles. *Nonlinear Dyn.*, 2013, **73**, pp 229–244.
[8] Sun H.B., Li S.H., Sun C.Y. and Wu L.G. Robust adaptive integral-sliding-mode fault-tolerant control for airbreathing hypersonic vehicles. *Proc. Inst. Mech. Eng. Part I: J. Syst. Control Eng.*, 2012, **226**, (10), pp 1344–1355.
[9] Yang J., Li S.H., Sun C.Y. and Guo L. Nonlinear-disturbance-observer-based robust flight control for airbreathing hypersonic vehicles. *IEEE Trans. Aerosp. Electron. Syst.*, 2013, **49**, (2), pp 1263–1275.
[10] Zhu P., Jiang J. and Yu C. Fault-tolerant control of hypersonic vehicles based on fast fault observer under actuator gain loss fault or stuck fault. *Aeronaut. J.*, 2020, **124**, (1278), pp 1190–1207.
[11] Yun Y., Tang S. and Guo J. Smooth adaptive fixed time convergent controller design for BTT missiles with uncertainties. *Aeronaut. J.*, 2020, **124**, (1273), pp 323–345.
[12] Han X., Liu L., Fan H.J. and Cheng Z.T. Robust approximate optimal control for air-breathing hypersonic vehicle. *Int. J. Robust Nonlinear Control*, 2023, **33**, (7), pp 4117–4140.
[13] Ilchmann A., Ryan E.P., Sangwin C.J. and Guo L. Tracking with prescribed transient behaviour. *ESAIM: Control Opt. Calc. Var.*, 2002, **7**, pp 471–493.
[14] Bechlioulis C.P., Rovithakis G.A., Sun C.Y. and Guo L. Robust adaptive control of feedback linearizable MIMO nonlinear systems with prescribed performance. *IEEE Trans. Autom. Control*, 2008, **53**, (9), pp 2090–2099.
[15] Shao X.D., Hu Q.L., Shi Y. and Jiang B.Y. Fault-tolerant prescribed performance attitude tracking control for spacecraft under input saturation. *IEEE Trans. Control Syst. Technol.*, 2018, **28**, (2), pp 574–582.
[16] Gao S.H., Liu X.P., Jing Y.W. and Dimirovski G.M. A novel finite-time prescribed performance control scheme for spacecraft attitude tracking. *Aerosp. Sci. Technol.*, 2021, **118**, pp 107044.
[17] Hua C.C., Chen J.N., Guan X.P. and Dimirovski G.M. Adaptive prescribed performance control of QUAVs with unknown time-varying payload and wind gust disturbance. *J. Franklin Inst.*, 2018, **355**, (14), pp 6323–6338.
[18] Bechlioulis C.P. and Rovithakis G.A. Decentralized robust synchronization of unknown high order nonlinear multi-agent systems with prescribed transient and steady state performance. *IEEE Trans. Autom. Control*, 2016, **62**, (1), pp 123–134.
[19] Bechlioulis C.P. and Rovithakis G.A. Prescribed performance adaptive control for multi-input multi-output affine in the control nonlinear systems. *IEEE Trans. Autom. Control*, 2010, **55**, (5), pp 1220–1226.
[20] Bu X.W., Wu X.Y., Zhu F.J., Huang J.Q., Ma Z. and Zhang R. Novel prescribed performance neural control of a flexible air-breathing hypersonic vehicle with unknown initial errors. *ISA Trans.*, 2015, **59**, pp 149–159.
[21] Bu X.W., Qi Q., Jiang B. and Huang J.Q. A simplified finite-time Fuzzy neural controller with prescribed performance applied to Waverider aircraft. *IEEE Trans. Fuzzy Syst.*, 2022, **30**, (7), pp 2529–2537.
[22] Wei C.S., Luo J.J., Yin Z.Y. and Yuan J.P. Leader-following consensus of second-order multi-agent systems with arbitrarily appointed-time prescribed performance, *IET Control Theory Appl.*, 2018, **12**, (16), pp 2276–2286.
[23] Liu Y., Li G., Li Y.C. and Wu Y.H. Novel prescribed performance control scheme for flexible hypersonic flight vehicles with nonaffine dynamics and neural approximation. *Int. J. Aerosp. Eng.*, 2021, **13**, pp 1–14.
[24] Zhu S.P., Xu T., Wei C.S. and Wang Z. Learning-based adaptive fault tolerant control for hypersonic flight vehicles with abrupt actuator faults and finite time prescribed tracking performance. *Eur. J. Control*, 2021, **58**, pp 17–26.
[25] Keshmiri S., Colgren R., Mirmirani M. and Bai R.Y. Six DoF nonlinear equations of motion for a generic hypersonic vehicle. *AIAA Atmospheric Flight Mech. Conf. Exhibit*, 20 August - 23 August, 2007, Hilton Head, South Carolina, America.
[26] Zhang C., Ma G.F., Sun Y.C. and Li C.J. Simple model-free attitude control design for flexible spacecraft with prescribed performance. *Proc. Inst. Mech. Eng. Part G: J. Aerosp. Eng.*, 2019, **233**, (8), pp 2760–2771.
[27] Wang W. and Wen C.Y. Adaptive actuator failure compensation control of uncertain nonlinear systems with guaranteed transient performance. *Automatica*, 2010, **46**, (12), pp 2082–2091.
[28] Bu X.W. Guaranteeing prescribed performance for air-breathing hypersonic vehicles via an adaptive non-affine tracking controller. *Acta Astronaut.*, 2018, **151**, pp 368–379.
[29] Bu X.W., Wu X.Y., Chen Y.X. and Bai R.Y. Design of a class of new nonlinear disturbance observers based on tracking differentiators for uncertain dynamic systems. *Int. J. Control Autom. Syst.*, 2015, **13**, (3), pp 595–602.
[30] Hao F., Zhang D., Cao L. and Tang S. Disturbance decoupling control for flexible air-breathing hypersonic vehicles with mismatched condition. *Asian J. Control*, 2019, **21**, (3) pp 1100–1110.
[31] Bu X.W., Wu X.Y., Zhang R., Ma Z. and Huang J.Q. Tracking differentiator design for the robust backstepping control of a flexible air-breathing hypersonic vehicle. *J. Franklin Inst.*, 2015, **352**, (4) pp 1739–1765.
[32] Hu Q.L., Shi Y.X. and Shao X.D. Adaptive fault-tolerant attitude control for satellite reorientation under input saturation. *Aerosp. Sci. Technol.*, 2018, **78**, pp 171–182.
[33] Hou M.Z., Liang X.L., Duan G.R. and Bai R.Y. Adaptive block dynamic surface control for integrated missile guidance and autopilot. *Chin. J. Aeronaut.*, 2013, **26**, (3) pp 741–750.

Cite this article: Yin Z.Y., Wang B., Xiong R.T., Xiang Z., Liu L., Fan H.J. and Xue C.L. (2024). Attitude tracking control of hypersonic vehicle based on an improved prescribed performance dynamic surface control. *The Aeronautical Journal*, **128**, 875–895. https://doi.org/10.1017/aer.2023.79